

See discussions, stats, and author profiles for this publication at: <https://www.researchgate.net/publication/265473778>

Graphene Nanopore with a Self-Integrated Optical Antenna

ARTICLE *in* NANO LETTERS · SEPTEMBER 2014

Impact Factor: 13.59 · DOI: 10.1021/nl503159d · Source: PubMed

CITATIONS

10

READS

213

8 AUTHORS, INCLUDING:



Inhee Choi

University of Seoul

62 PUBLICATIONS 942 CITATIONS

[SEE PROFILE](#)



Yeonho Choi

Korea University

37 PUBLICATIONS 758 CITATIONS

[SEE PROFILE](#)



Luke P Lee

University of California, Berkeley

303 PUBLICATIONS 9,954 CITATIONS

[SEE PROFILE](#)

Graphene Nanopore with a Self-Integrated Optical Antenna

SungWoo Nam,^{†,‡,○} Inhee Choi,^{†,‡,□} Chi-cheng Fu,^{†,‡} Kwanpyo Kim,^{§,||,⊥} SoonGweon Hong,^{†,‡} Yeonho Choi,[#] Alex Zettl,^{§,||,⊥} and Luke P. Lee^{*†,‡,○,V,■}

[†]Department of Bioengineering, [‡]Berkeley Sensor and Actuator Center, [§]Department of Physics, ^{||}Center of Integrated Nanomechanical Systems, ^VDepartment of Electrical Engineering and Computer Sciences, and [■]Biophysics Graduate Program, University of California, Berkeley, California 94720, United States

[#]Materials Sciences Division, Lawrence Berkeley National Laboratory, Berkeley, California 94720, United States

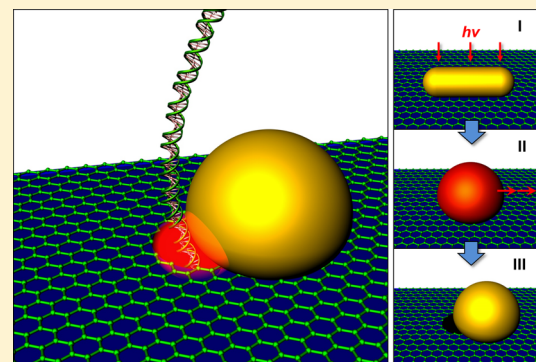
^{*}Department of Biomedical Engineering, Korea University, Seoul 136-701, Republic of Korea

[○]Department of Mechanical Science and Engineering, University of Illinois, Urbana-Champaign, Urbana, Illinois 61801, United States

[□]Department of Life Science, University of Seoul, Seoul 130-743, Republic of Korea

S Supporting Information

ABSTRACT: We report graphene nanopores with integrated optical antennae. We demonstrate that a nanometer-sized heated spot created by photon-to-heat conversion of a gold nanorod resting on a graphene membrane forms a nanoscale pore with a self-integrated optical antenna in a single step. The distinct plasmonic traits of metal nanoparticles, which have a unique capability to concentrate light into nanoscale regions, yield the significant advantage of parallel nanopore fabrication compared to the conventional sequential process using an electron beam. Tunability of both the nanopore dimensions and the optical characteristics of plasmonic nanoantennae are further achieved. Finally, the key optical function of our self-integrated optical antenna on the vicinity of graphene nanopore is manifested by multifold fluorescent signal enhancement during DNA translocation.



KEYWORDS: Self-organized formation, graphene, nanopore, optical antennae, DNA translocation, fluorescence enhancement

The atomically thin nature of graphene^{1–3} makes it an ideal translocation membrane for high resolution, high throughput, single-molecule DNA sequencing based on nanopores.^{4–7} The conventional approach to creating nanopores on graphene requires a high-resolution electron beam sculpting/drilling process,^{4–9} which often suffers from process variability, precluding the platform from being scalable. Here, we report the formation of graphene nanopores with self-integrated optical antennae in a single step by parallel photothermal sculpting. We show that a nanometer-sized heated spot created by photon-to-heat conversion^{10–13} (i.e., photothermal effect) of a gold nanorod resting on a graphene membrane forms a nanoscale pore with a self-integrated optical nanoantenna in a single step. The unique interface of graphene nanopore–plasmonic optical antenna is composed of a nanopore with a smallest achievable dimension of a few nanometers and a hemispherically shaped gold nanoparticle located adjacent to the nanopore. The distinct plasmonic traits of metal nanoparticles, which concentrate micron-sized light into nanoscale regions, yield the significant advantage of parallel nanopore fabrication compared to the conventional sequential process using an electron beam. In addition, we achieve tunability of both the nanopore dimensions and the optical characteristics of plasmonic nanoantennae by controlling laser fluence and the

dimension of nanoparticles. Finally, the optical function of our self-integrated plasmonic nanoantenna on graphene nanopore is manifested by multifold fluorescent signal enhancement during single lambda phage DNA translocation through a graphene nanopore. We believe our simple approach to forming a self-integrated graphene nanopore and optical antenna could potentially offer a new avenue and advances for nanopore-based simultaneous electrical and optical DNA sequencing.^{8,9,14–16}

Figure 1a shows an artist representation of the graphene nanopore sensor with a self-integrated optical nanoantenna. Similar to conventional solid-state nanopores,^{8,15} a nanoscale pore on an atomically thin graphene membrane is the fulcrum for the translocation of biomolecules. The unconventional component of our sensor architecture is the integrated optical antenna on the graphene nanopore, which acts as an optical transducer (or optical signal enhancer) to complement standard ion current measurements.

Our one-step photothermal formation strategy of graphene nanopores with self-integrated optical antennae is illustrated in

Received: June 3, 2014

Published: September 2, 2014

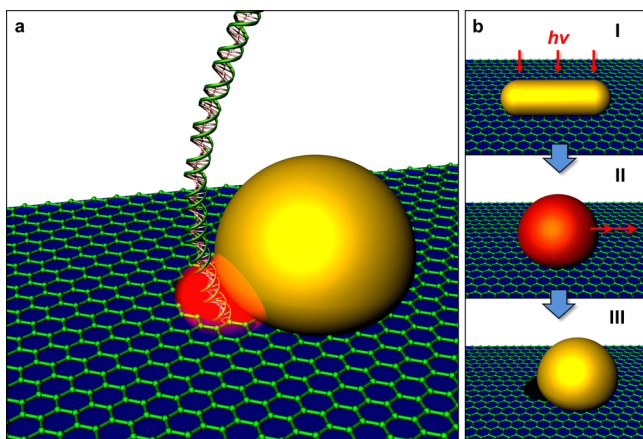


Figure 1. Schematic drawing of graphene nanopore with self-integrated optical antenna. (a) Schematic illustration of DNA translocation event through graphene nanopore with self-integrated optical antenna (gold) and enhanced optical signal (red) at the junction of nanopore and optical antenna. Nanoscale optical antenna functions as optical signal transducer and enhancer. (b) Illustration of photothermal sculpting process of graphene nanopores: (I) Light ($h\nu$) is illuminated on a gold nanorod on a graphene membrane, (II) the gold nanorod is melted and reshaped into a hemispherical nanoparticle (red color indicates a high surface temperature), and (III) the heated gold nanoparticle subsequently oxidizes the graphene surface to create a nanopore.

Figure 1b. Graphene is synthesized^{17–19} and transferred²⁰ onto a holey-carbon grid or an ultrathin carbon membrane. Gold nanorods are then drop-cast on freestanding graphene or graphene resting on an ultrathin carbon membrane (see Methods). The sample of nanoparticles on graphene is illuminated with light ($h\nu$) of wavelength matching the peak of resonant absorbance of gold nanoparticles (I in Figure 1b). For example, maximum absorption for gold nanorods with short and long dimensions of 10 and 38 nm, respectively, occurs at a wavelength of ~800 nm. During light illumination with a femto-second laser, photon-to-heat conversion (i.e., a photothermal effect) causes gold nanorods to reach a temperature around its melting point and results in a heated spot formation at the nanoparticle (II in Figure 1b). For a single laser pulse fluence of 2 mJ/cm², simulation results (Figure S3, Supporting Information) show that the nanoparticle reaches a maximum temperature of up to 680 °C (in about 140 fs) and cools down to room temperature (in about 10 ps). Gold nanorods heated close to the melting temperature then become mobile (under radiation force) to generate nanopores with controllable dimensions (III in Figure 1b). Our estimation shows that radiation forces alone could induce directional nanoparticle movement in the order of 100 nm (see the Supporting Information). The nanopores are created because the local temperature around heated and mobile nanoparticles exceeds the oxidation temperature of the graphene membrane²¹ in an atmospheric environment.

To demonstrate the capability of our parallel photon-to-heat sculpting of nanopores on graphene using plasmonic nano-

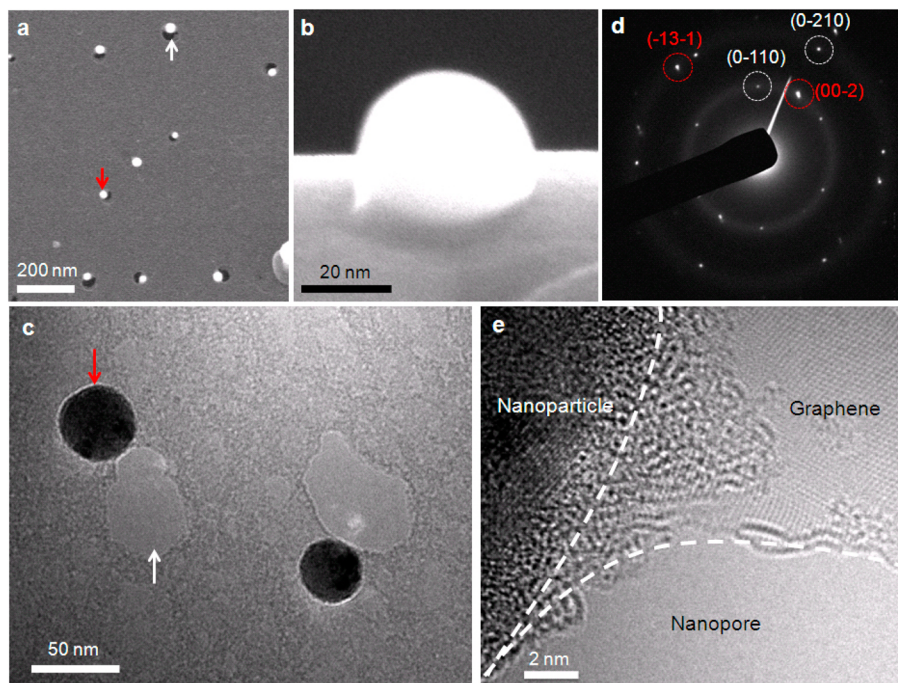


Figure 2. Electron microscope characterization of graphene nanopores with self-integrated optical antennae. (a) SEM image of nanopores formed on graphene on an ultrathin carbon membrane. Each gold nanoparticle (appearing white, red arrow) is self-integrated at the vicinity of nanopore (appearing black, white arrow). A single poration event yields an array of graphene nanopores with integrated optical nanoantennae. (b) Side-view SEM of a gold nanorod after light illumination, showing a hemispherically shaped gold nanoparticle. (c) TEM image of two nanopores simultaneously formed by photon-to-heat sculpting. Gold nanoparticles (appearing black, red arrow) are integrated at the vicinity of nanopores (appearing white, white arrow) with a nanopore diameter of ~50 nm. (d) Electron diffraction pattern taken from the gold nanoantenna on a graphene membrane. Diffraction pattern of a gold nanoparticle indexed as the [310] zone axis of face centered cubic (indexed in red) with a set of hexagonal patterns from single-layer graphene (indexed in white). (e) Atomic resolution TEM image of the graphene nanopore-optical nanoantenna interface. White dashed lines indicate nanoparticle-graphene and graphene-nanopore interfaces.

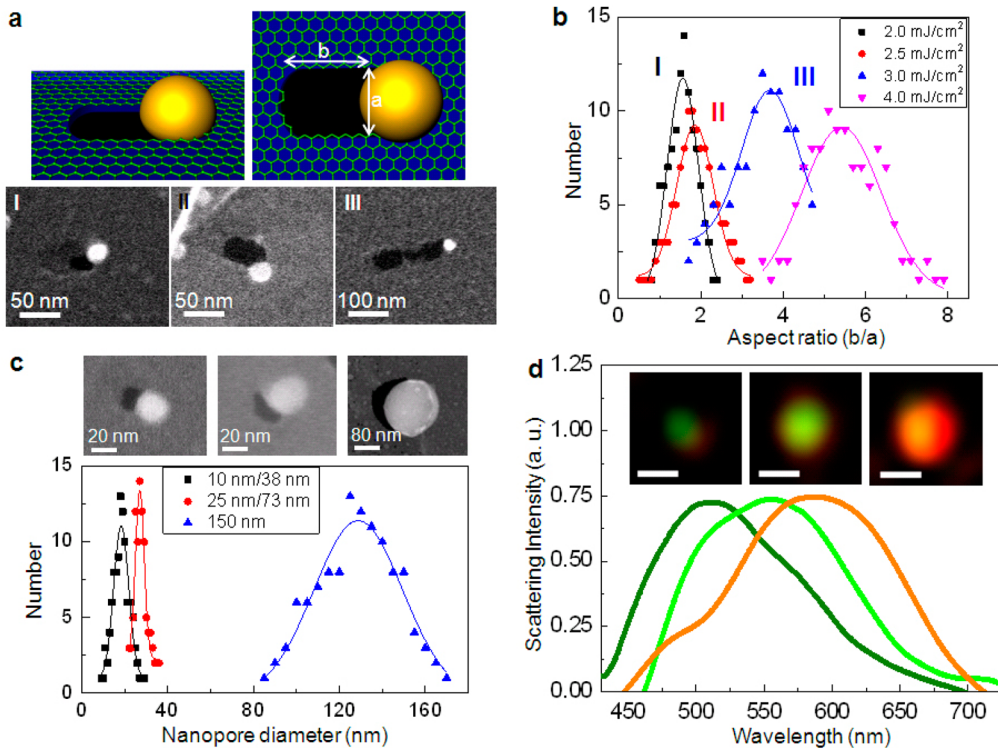


Figure 3. Shape and size tunability of photon-to-heat graphene nanopore sculpting and corresponding plasmonic characteristics. (a) Schematic illustration of nanopore anisotropy (b/a). The length (b) of a nanopore and the diameter of a gold nanoparticle (a) are used to define the anisotropy of the nanopore. SEM images (I, II, and III) of nanopores created at different laser illumination fluences in part b. (b) Statistical analysis of nanopore aspect ratio as a function of laser fluence. (c) Statistical distribution of nanopore diameter created with three different sizes of gold nanoparticles: (10 nm × 38 nm) and (25 nm × 73 nm) (short by long axis length) gold nanorods and 150 nm diameter gold nanospheres. The inset shows representative SEM images of graphene nanopores with integrated nanoparticles. (d) Darkfield scattering images and corresponding spectrum of plasmonic nanoparticles taken from nanopores with self-integrated nanoantennae in part c. Scale bar, 0.5 μm.

particles, we present scanning electron microscope (SEM) images of multiple nanopores created simultaneously on graphene on an ultrathin carbon membrane (c.a. 20 nm in thickness) in Figure 2a and Figure S4 (Supporting Information; pores appear black in both images). Atomic force microscopy characterizations of graphene nanopore with an integrated optical antenna (Figure S5, Supporting Information) further demonstrate parallel photo-to-heat sculpting of nanopores. As evident from these results, light illumination, with a laser pulse fluence of ~1.5 mJ/cm², at the peak absorption wavelength of gold nanorods is sufficient to create multiple nanopores at each location. Furthermore, nanorods undergo reshaping to a hemispherical form as shown in Figure 2b. For comparison, we show in Figure S6 (Supporting Information) a representative image of gold nanorods on a graphene/carbon membrane prior to illumination. We also observed that the shape change from nanorods to hemispheres occurs at a laser fluence as low as 0.5 mJ/cm², while the fluence for pore formation is ≥1.5 mJ/cm². Such nanopore formation (poration) by photon-to-heat sculpting is also observed in freestanding graphene membranes as shown in Figure S7 (Supporting Information) and Figure 2e. We note that graphene without a supporting substrate (freestanding graphene) is relatively less stable compared to graphene on a carbon membrane under laser illumination²² leading to damage of the membrane regardless of the presence of nanoparticles.

Transmission electron microscope (TEM) analysis of graphene nanopores with self-integrated optical nanoantennae is presented in Figure 2c–e. A TEM image of two graphene

nanoantennae clearly shows that c.a. 50 nm sized pores are created by photothermal sculpting (marked with a white arrow in Figure 2c) and that gold nanoparticles (marked with a red arrow) are located at the nanopores. We further show that by fine-tuning laser illumination condition we are able to obtain 2 nm wide and 60 nm long nanopores as shown in Figure S8 (Supporting Information). SEM energy dispersive analysis (Figure S9, Supporting Information) and selected area electron diffraction (Figure 2d) are performed to confirm and evaluate the crystallinity of gold nanoparticles after light illumination. Finally, an atomic resolution TEM image of graphene nanopore-optical nanoantenna interface is demonstrated in Figure 2e. The edge nanostructure of a graphene nanopore²³ is further studied through atomic resolution TEM (Figure S10, Supporting Information), which shows a graphene hexagonal lattice with a nanometer edge roughness created by photothermal sculpting.

To explore the tunability of photon-to-heat nanopore sculpting, we investigate the effect of laser illumination fluence on nanopore dimensions (Figure 3a and b). To systematically carry out the study, we use graphene on an ultrathin carbon membrane with 10 nm × 38 nm gold nanorods as a standard sample. First, at <1.5 mJ/cm² illumination fluence, we only observe reshaping of gold nanorods without any existence of nanopores. When the illumination fluence is ≥1.5 mJ/cm², we are able to observe that nanopores form with integrated gold nanoparticles and the aspect ratio (b/a) of nanopores changes with the illumination fluence. More specifically, statistical studies of illumination fluence and the aspect ratio of nanopore

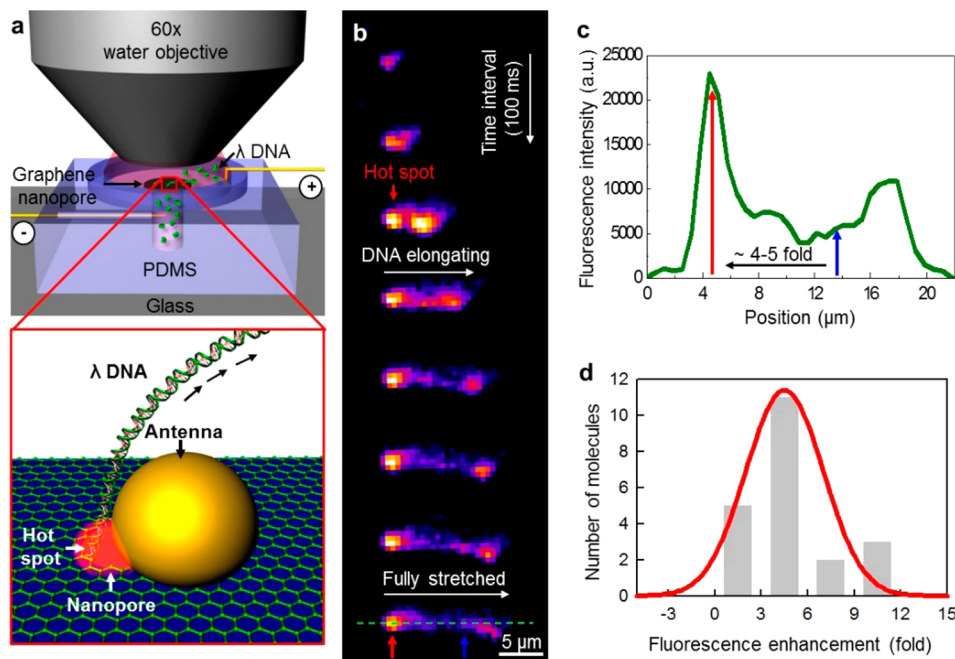


Figure 4. DNA translocation through integrated graphene nanopores with optical antennae. (a) Schematic drawing of a PDMS device mounted with an array of graphene nanopores with integrated nanoantennae. The inset shows a zoom-in view of plasmonically enhanced fluorescence of a stained λ DNA when passing through a graphene nanopore with an optical nanoantenna. (b) A time series of confocal scanning fluorescence images of λ DNA translocation with a time interval of 100 ms. The last image shows the DNA fully stretched by the applied electrical field at 800 ms. (c) Fluorescent intensity profile along the green dashed line in part b. Red and blue arrows indicate intensities at nanopore and the center points of a stretched DNA, respectively. (d) Histogram of the plasmonic fluorescent enhancement factor.

in Figure 3b clearly present an interesting trend. The aspect ratio of nanopores, or the travel distance of heated nanoparticles, grows as the illumination fluence increases, resulting in anisotropic nanopores (b/a of ~ 5.5) when the laser fluence is around 4 mJ/cm^2 . Our observation supports the pore formation mechanism by which the gold nanoparticle becomes increasingly mobile as more energy is absorbed by the nanoparticle. Furthermore, at laser fluences between 5 and 8 mJ/cm^2 (to remain below the threshold in which the graphene/carbon membrane is photodamaged), we note that, although anisotropic nanopores are detected, gold nanoparticles start to disappear, which is a key contrast to the results at lower intensities. Such findings demonstrate that, beyond a certain level of fluence, nanoparticles start to leave the graphene surface as optical pressure becomes higher than the surface tension/interaction.^{24,25} We highlight that the unique ability to adjust the shape of the nanopores could provide an interesting biophysical platform to study translocation events dependent on the shapes (i.e., isotropic versus anisotropic) of biomolecules.

In addition to shape tunability, we show that the diameter of nanopores can also be controlled by changing the size of the nanoparticles (Figure 3c). Here we fix our illumination fluence at 2 mJ/cm^2 and vary the initial nanoparticle dimensions. We use three different sizes of gold nanoparticles: (10 nm \times 38 nm) and (25 nm \times 73 nm) (short by long axis length) gold nanorods and 150 nm diameter gold nanospheres. As each type of nanoparticle has different absorption characteristics, we vary the illumination wavelength to match its respective peak absorption bands. We observe, consistent with earlier results, that each type of nanoparticle creates a nanopore with a diameter proportional to the initial dimensions of the nanoparticles after light illumination (Figure 3c). As the

nanoparticles melt prior to nanopore formation (Figure 1b), the nanopore diameter is determined by the size of nanoparticles after the reshaping step. It should be noted that there is no intrinsic limit of the nanoparticle size for the poration, if nanoparticle can absorb the light at their excitation wavelength and we can use compatible laser source with the absorption band of nanoparticle.

One unique aspect of our nanopore fabrication approach is that the optical antennae with tunable plasmonic characteristics are readily integrated with the nanopores. To illustrate this feature, we perform dark-field imaging (Figure 3d) of integrated optical nanoantennae of three different dimensions in Figure 3c. Scattering images show dark green, bright green, and orange colors (left to right, insets in Figure 3d) taken from graphene nanopores with plasmonic nanoparticles of differing diameters, consistent with previous reports in the literature²⁶ where a red-shift of plasmon resonance occurs as the size of nanoparticles increases. Corresponding spectrum analysis shows scattering peaks of 510, 550, and 590 nm from the three different nanoparticle dimensions, respectively. We believe that the tunability of optical characteristics could allow for future multiplexed optical detection/sequencing.

We have explored optical features of our graphene nanopores with self-integrated optical antennae platform during DNA translocation events.²⁷ Lambda (λ) DNA (48.50 kbp) molecules are labeled with green fluorescence dyes (TOTO-1). The DNA sample and buffer solution are injected into the bottom chamber and the top reservoir respectively of a polydimethylsiloxane (PDMS) electrophoresis device mounted with an array of graphene nanopores and integrated optical antennae (Figure 4a and Figure S1, Supporting Information). The dynamics of DNA translocation through graphene nanopores is recorded by a water immersion objective lens

equipped on a fluorescent microscope. Gold nanoantennae on the edge of nanopores have a surface plasmon resonance peak at 510 nm (Figure 3d), which overlaps well with the absorption peak of TOTO-1, ensuring resonant interactions and metal-enhanced fluorescence (inset of Figure 4a).²⁸

When DNA molecules pass through the nanopore under an electrical field, we observe a bright fluorescent spot at the nanopore. The bright spot maintains its intensity during the entire elongation and stretching process (Figure 4b), and finally, the λ DNA is nearly fully stretched to $\sim 18 \mu\text{m}$ with minimal partial coiling. The localized heating at the proximity of Au nanoantenna could lead to stretched conformations of DNA via thermophoretic forces^{29,30} as observed in Figure 4b. We note that fluorescent imaging is less sensitive to translocation events due to the finite focal volume of imaging,^{27,31,32} and furthermore plasmonic trapping effects of the integrated Au nanoantenna might further enhance the dwelling time of DNA at around the nanopore.³³

Detailed analysis of the fluorescent intensity profile from fully stretched DNA (Figure 4c) shows that the fluorescence intensity is 4 to 5-fold higher at the nanopore (red arrow) than at the center (blue arrow), as shown in Figure 4b and c. The enhanced fluorescence is observed reproducibly for the subsequent studies, as seen in histograms of enhancement factors, showing a peak centered at 4.5 times in Figure 4d. Such observations, in contrast to the results of nanopores without any optical nanoantennae (Figure S11, Supporting Information), clearly demonstrated that the plasmonic optical nanoantenna enhances single-molecule fluorescence.²⁸ We note that our approach is also applicable to conventional ionic current measurements of translocation events by creating a single nanopore (by positioning a single Au nanoparticle on graphene translocation membrane) and subsequent integration of the translocation chamber and measurement electrode.⁸

Our photon-to-heat sculpting of nanopores presents numerous advantages over the conventional direct atomic displacement approach as well as new capabilities. First, photon-to-heat sculpting allows simple and inexpensive nanopore creation by utilizing nanoplasmatic photothermal effects at well below the diffraction limit, thus eliminating the need for high-end electron microscopy (Table S1, Supporting Information). Second, parallel nanopore creation is an intrinsic feature of our photon-to-heat poration, whereas the nanopores are formed sequentially in conventional electron beam sculpting.⁸ Third, photothermal-sculpting spanning up to a few nanometers surrounding the plasmonic nanoparticle^{11,34} has fewer potential defects that can arise during the poration process compared to electron beam sculpting because it does not expose the sample to electron beams at high acceleration voltages.^{4–9} Fourth, our readily integrated optical nanoantennae serve new and unique functions, which are useful to plasmonic sensors and transducers with high-throughput nanopore platforms.¹³ For example, hot-spot-mediated surface enhancements have gained considerable attention recently because of their ability to lower the detection thresholds and also improve the spatial and temporal resolution.^{35,36} In addition, strong light-to-force conversion based on plasmonic hotspots has the potential to facilitate single molecular manipulations (e.g., nanoplasmatic trapping).^{33,37,38} A significantly strong and nanometer-sized hot spot,³⁹ together with the high throughput and fine nanofluidic control over reagents with nanopore techniques, makes our novel integrated material a promising platform for ultrasensitive and ultrafast detection for

biomedical applications. Finally, the metallic surfaces of the nanoantennae could facilitate functionalization of biomolecules,^{34,40} enabling enzymatic separation/unzipping of double-stranded DNA⁴¹ without any need to perturb the inert surface of the graphene membrane.¹⁷

In conclusion, we have developed a novel yet simple approach to create graphene nanopores with self-integrated optical antennae by photothermal conversion. We show that the unique interface of graphene nanopore-optical antenna is formed with the smallest graphene nanopore width of $\sim 2 \text{ nm}$ and a hemispherically shaped gold nanoparticle spontaneously integrated at the nanopore. Furthermore, we realize the tunability of nanopore shape and dimension by controlling laser illumination fluence and size of initial nanoparticles, respectively. Plasmonic resonance characteristics of self-integrated nanoantennae are also controllable for potential multiplexed optical detection as demonstrated by the fluorescent signal enhancement during λ DNA translocation through graphene nanopores. We believe our new approach to forming self-integrated optical antennae adjacent to graphene nanopores could pave the way toward hybrid optical and electrical DNA sequencing based on nanopore technology with the regulation of DNA translocation in the future.

Methods. Graphene was synthesized by copper-catalyzed chemical vapor deposition and transferred onto a holey carbon grid or an ultrathin carbon membrane described previously.^{18–20} Gold nanoparticles (10^{11} particles/mL; Nanopartz Inc.) are then drop-casted followed by exposure to light illumination ($h\nu$) with its wavelength matching the peak absorbance of gold nanoparticles. Femto-second laser (80 MHz repetition rate, 140 fs pulse width; Chameleon Ultra II, Coherent) was used with a fluence range of 0.5–10 mJ/cm². SEM and TEM analyses were performed to investigate nanopore formation and to measure the dimensions of the nanopore. Dark-field microscopy (Carl Zeiss Axiovert 200 inverted microscope with dry darkfield condenser) with spectrum analysis (Acton Research) was carried out to characterize plasmonic properties of integrated gold nanoantennae. An aperture was placed at the entrance slit of the monochromator (few-micron-wide aperture) to obtain a spectrum solely from a single nanoparticle in the region of interest. A DNA translocation experiment was performed with fluorescently labeled λ DNA (TOTO-1; Molecular Probes), and fluorescent images were recorded during DNA translocation by a confocal microscope.

■ ASSOCIATED CONTENT

● Supporting Information

Detailed methods and supporting figures. This material is available free of charge via the Internet at <http://pubs.acs.org>.

■ AUTHOR INFORMATION

Corresponding Author

*L.P.L. E-mail: lplee@berkeley.edu.

Author Contributions

S.W.N., I.C., and C.-C.F. contributed equally. L.P.L. conceived the integrated graphene nanopore with plasmonic optical antenna for simultaneous direct optical DNA sequence detection and electrical signal cross-correlation. L.P.L., and S.W.N. designed experiments. S.W.N., I.C., and C.-C.F. performed experiments, and K.K., and A.Z. contributed to

graphene preparation. S.W.N., I.C., C.-C.F., and L.P.L. prepared the manuscript.

Notes

The authors declare no competing financial interest.

ACKNOWLEDGMENTS

L.P.L. acknowledges support from Samsung Electronics, Inc., and thanks the Advanced Characterization Center of Yonsei Institute of Convergence Technology for providing their support in the AFM characterization. A.Z. and K.K. acknowledge support from the Director, Office of Energy Research, Office of Basic Energy Sciences, Materials Sciences and Engineering Division, of the U.S. Department of Energy under Contract No. DE-AC02-05CH11231 which provided for TEM characterization, and the National Science Foundation within the Center of Integrated Nanomechanical Systems which provided for graduate student support and under grant no. DMR-1206512 which provided support for graphene synthesis and transfer.

REFERENCES

- (1) Novoselov, K. S.; Geim, A. K.; Morozov, S. V.; Jiang, D.; Katsnelson, M. I.; Grigorieva, I. V.; Dubonos, S. V.; Firsov, A. A. *Nature* **2005**, *438*, 197–200.
- (2) Zhang, Y.; Tan, Y.; Stormer, H. L.; Kim, P. *Nature* **2005**, *438*, 201–204.
- (3) Novoselov, K. S.; Geim, A. K.; Morozov, S. V.; Jiang, D.; Zhang, Y.; Dubonos, S. V.; Grigorieva, I. V.; Firsov, A. A. *Science* **2004**, *306*, 666–669.
- (4) Garaj, S.; Hubbard, W.; Reina, A.; Kong, J.; Branton, D.; Golovchenko, J. A. *Nature* **2010**, *467*, 190–193.
- (5) Schneider, G. F.; Kowalczyk, S. W.; Calado, V. E.; Pandraud, G.; Zandbergen, H. W.; Vandersypen, L. M. K.; Dekker, C. *Nano Lett.* **2010**, *10*, 3163–3167.
- (6) Merchant, C. A.; Healy, K.; Wanunu, M.; Ray, V.; Peterman, N.; Bartel, J.; Fischbein, M. D.; Venta, K.; Luo, Z.; Johnson, A. T. C.; Drndić, M. *Nano Lett.* **2010**, *10*, 2915–2921.
- (7) Venkatesan, B. M.; Estrada, D.; Banerjee, S.; Jin, X.; Dorgan, V. E.; Bae, M.-H.; Aluru, N. R.; Pop, E.; Bashir, R. *ACS Nano* **2012**, *6*, 441–450.
- (8) Dekker, C. *Nat. Nanotechnol.* **2007**, *2*, 209–215.
- (9) Xie, P.; Xiong, Q.; Fang, Y.; Qing, Q.; Lieber, C. M. *Nat. Nanotechnol.* **2012**, *7*, 119–125.
- (10) Cao, L.; Barsic, D. N.; Guichard, A. R.; Brongersma, M. L. *Nano Lett.* **2007**, *7*, 3523–3527.
- (11) Fedoruk, M.; Lutich, A. A.; Feldmann, J. *ACS Nano* **2011**, *5*, 7377–7382.
- (12) Liu, G. L.; Kim, J.; Lu, Y.; Lee, L. P. *Nat. Mater.* **2006**, *5*, 27–32.
- (13) Jain, P. K.; Huang, X.; El-sayed, I. H.; El-sayed, M. A. *Acc. Chem. Res.* **2008**, *41*, 1578–1586.
- (14) Pennisi, E. *Science* **2012**, *336*, 534–537.
- (15) Venkatesan, B. M.; Bashir, R. *Nat. Nanotechnol.* **2011**, *6*, 615–624.
- (16) Branton, D.; Deamer, D. W.; Marziali, A.; Bayley, H.; Benner, S. A.; Butler, T.; Ventra, M. D.; Garaj, S.; Hibbs, A.; Huang, X.; Jovanovich, S. B.; Krstic, P. S.; Lindsay, S.; Ling, X. S.; Mastrangelo, C. H.; Meller, A.; Oliver, J. S.; Pershin, Y. V.; Ramsey, J. M.; Riehn, R.; Soni, G. V.; Tabard-Cossa, V.; Wanunu, M.; Wiggin, M.; Schloss, J. A. *Nat. Biotechnol.* **2008**, *26*, 1146–1153.
- (17) Geim, A. K. *Science* **2009**, *324*, 1530–1534.
- (18) Li, X.; Cai, W.; An, J.; Kim, S.; Nah, J.; Yang, D.; Piner, R.; Velamakanni, A.; Jung, I.; Tutuc, E.; Banerjee, S. K.; Colombo, L.; Ruoff, R. S. *Science* **2009**, *324*, 1312–1314.
- (19) Bae, S.; Kim, H.; Lee, Y.; Xu, X.; Park, J.-S.; Zheng, Y.; Balakrishnan, J.; Lei, T.; Kim, H. R.; Song, Y. I.; Kim, Y.-J.; Kim, K. S.; Özyilmaz, B.; Ahn, J.-H.; Hong, B. H.; Iijima, S. *Nat. Nanotechnol.* **2010**, *5*, 574–578.
- (20) Regan, W.; Alem, N.; Alemán, B.; Geng, B.; Girit, C.; Maserati, L.; Wang, F.; Crommie, M.; Zettl, A. *Appl. Phys. Lett.* **2010**, *96*, 113102–113102.
- (21) Liu, L.; Ryu, S.; Tomasik, M. R.; Stolyarova, E.; Jung, N.; Hybertsen, M. S.; Steigerwald, M. L.; Brus, L. E.; Flynn, G. W. *Nano Lett.* **2008**, *8*, 1965–1970.
- (22) Yoo, J.-H.; In, J. B.; Park, J. B.; Jeon, H.; Grigopoulos, C. P. *Appl. Phys. Lett.* **2012**, *100*, 233124–233124.
- (23) Girit, C. O.; Meyer, J. C.; Erni, R.; Rossell, M. D.; Kisielowski, C.; Yang, L.; Park, C.-H.; Crommie, M. F.; Cohen, M. L.; Louie, S. G.; Zettl, A. *Science* **2009**, *323*, 1705–1708.
- (24) Habenicht, A.; Olapinski, M.; Burmeister, F.; Leiderer, P.; Boneberg, J. *Science* **2005**, *309*, 2043–2045.
- (25) Nedev, S.; Urban, A. S.; Lutich, A. A.; Feldmann, J. *Nano Lett.* **2011**, *11*, 5066–5070.
- (26) Ross, B. M.; Lee, L. P. *Opt. Lett.* **2009**, *34*, 896–898.
- (27) Chansin, G. A. T.; Mulero, R.; Hong, J.; Kim, M. J.; deMello, A. J.; Edel, J. B. *Nano Lett.* **2007**, *7*, 2901–2906.
- (28) Zhang, J.; Fu, Y.; Chowdhury, M. H.; Lakowicz, J. R. *Nano Lett.* **2007**, *7*, 2101–2107.
- (29) Jonsson, M. P.; Dekker, C. *Nano Lett.* **2013**, *13*, 1029–1033.
- (30) Belkin, M.; Maffeo, C.; Wells, D. B.; Aksimentiev, A. *ACS Nano* **2013**, *7*, 6816–6824.
- (31) Thacker, V. V.; Ghosal, S.; Hernández-Ainsa, S.; Bell, N. A. W.; Keyser, U. F. *Appl. Phys. Lett.* **2012**, *101*, 223704.
- (32) Kurz, V.; Nelson, E. M.; Shim, J.; Timp, G. *ACS Nano* **2013**, *7*, 4057–4069.
- (33) Juan, M. L.; Righini, M.; Quidant, R. *Nat. Photonics* **2011**, *5*, 349–356.
- (34) Lee, S. E.; Liu, G. L.; Kim, F.; Lee, L. P. *Nano Lett.* **2009**, *9*, 562–570.
- (35) Cang, H.; Labno, A.; Lu, C.; Yin, X.; Liu, M.; Gladden, C.; Liu, Y.; Zhang, X. *Nature* **2011**, *469*, 385–388.
- (36) Kinkhabwala, A.; Yu, Z.; Fan, S.; Avlasevich, Y.; Mullen, K.; Moerner, W. E. *Nat. Photonics* **2009**, *3*, 654–657.
- (37) Grigorenko, A. N.; Roberts, N. W.; Dickinson, M. R.; Zhang, Y. *Nat. Photonics* **2008**, *2*, 365–370.
- (38) Pang, Y.; Gordon, R. *Nano Lett.* **2012**, *12*, 402–406.
- (39) Thacker, V. V.; Herrmann, L. O.; Sigle, D. O.; Zhang, T.; Liedl, T.; Baumberg, J. J.; Keyser, U. F. *Nat. Commun.* **2014**, *5*, 3448.
- (40) Park, S. Y.; Lytton-Jean, A. K. R.; Lee, B.; Weigand, S.; Schatz, G. C.; Mirkin, C. A. *Nature* **2008**, *451*, 553–556.
- (41) Manrao, E. A.; Derrington, I. M.; Laszlo, A. H.; Langford, K. W.; Hopper, M. K.; Gillgren, N.; Pavlenok, M.; Niederweis, M.; Gundlach, J. H. *Nat. Biotechnol.* **2012**, *30*, 349–353.